Vol. 43, No. 1 (2021) 23-39, DOI: 10.24874/ti.952.08.20.01

Tribology in Industry

www.tribology.rs

RESEARCH

Mechanical and Tribological Properties Evolution of $[Si_3N_4/Al_2O_3]n$ Multilayer Coatings

C.H. Ortiz[a,*], E. Hernandez-Rengifo[a], A. Guerrero[a], W. Aperador[b], J.C. Caicedo[a]

[a]*Tribology, Powder Metallurgy and Processing of Solid Recycled Research Group, Universidad del Valle, Cali, Colombia,*
[b]*Universidad Militar Nueva Granada, Bogotá, Colombia.*

Keywords:

Physical vapor deposition PVD
Mechanical properties
Multilayer coatings
Friction coefficient
Lubricated tribological properties

* Corresponding author:

Christian Ortiz Ortiz
Christian.ortiz.ortiz@correounivalle.edu.co

Received: 28 August 2020
Revised: 12 October 2020
Accepted: 8 January 2021

A B S T R A C T

Multilayer coatings $[Si_3N_4/Al_2O_3]_n$ have generated great interest due to their intriguing properties which have made them a potential candidate to be implemented in different processes within the food and pharmaceutical industries. Unfortunately, this multilayer system based on $[Si_3N_4/Al_2O_3]_n$ does not have strong tribological studies that could express in an emphatic way its own tribological characteristics. For this reason, the aim of this research consisted of a detailed study of the evolution of the mechanical and tribological properties of the $[Si_3N_4/Al_2O_3]_n$ coatings as a function of the bilayer number n=1, 10, 30 and 70, with special emphasis on the tribological analysis in a dry and lubricated environment. It was determined that the mechanical properties such as the hardness and the elastic modulus increased by 29% and 6.3%, while the friction coefficient in a dry and lubricated environment decreased by 33% and 81.8%, respectively, when increasing the bilayers from n=1 to n=70. Thus, the present study determined that the coating $[Si_3N_4/Al_2O_3]_{70}$ presented ideal properties that make it a promising candidate to be implemented as a protective coating on processing devices within the food and pharmaceutical industry.

© 2021 Published by Faculty of Engineering

1. INTRODUCTION

Continuous industrial demand at a global scale, as well as competitiveness within industries, requires the incorporation of high performance materials to minimize energy loss and to be economically effective [1,2]. Therefore, it is necessary to design tribologically compatible coatings with high wear resistance and low friction, which are able to withstand aggressive environments and provide longer service life to the parts or tools coated with the single layers and multilayers coatings [3-10]. In literature, many single layer coating materials with the purpose of increasing mechanical properties have been reported such as Si_3N_4, which has been used in various applications within the metalworking industry due to its high resistance, low thermal conductivity and inter chemical

behavior in aggressive environments [11, 12]. Another single layer coating material reported is Al_2O_3, which possesses high hardness, high chemical stability and refractory characteristics. This material is commonly used on surface that are exposed to frictional wear and erosion by solid particles, as well as surfaces exposed to high temperatures [13]. However, literature has shown that there is substantial improvements when multilayer systems are developed instead of conventional single layer system such as $[HfV/VN]_n$ [14], $[TiN/ZrN]_n$ [15], $[TiN/TiAlN]_n$ [16], among other multilayers [17-20], bringing together the best characteristics of multiple layers. One example of these characteristics their multilayer structure, which by presenting symmetry breaks between each layer, a resistance to crack propagation is generated, increasing the mechanical and tribological properties. Currently, the multilayer systems $[Si_3N_4/Al_2O_3]n$ has generated great interest due to its high mechanical, morphological and tribological properties, which have made it a potential candidate to be used as a protective coating in processing equipment and cutting tools within different industries. Nevertheless, this multilayer system does not have strong tribological studies, that demonstrate the capabilities and particular characteristics of this system when in contact with other types of materials. In the same way, there is no evidence of tribological studies in different types of environments such as lubricated environments, high temperature environments, among others. Therefore, the aim of this research was focused on expanding the knowledge about the mechanical properties such as hardness and elastic modulus and mainly the tribological properties in a dry and lubricated environment of $[Si_3N_4/Al_2O_3]n$ multilayer coatings as a function of the bilayer number n=1, 10, 30 and 70. As a result, a scientific basis determining that the multilayer coating is a promising material to be implemented within the food and pharmaceutical industries was obtained.

2. EXPERIMENTAL SECTION

2.1 Materials

The AISI 316 steel substrates were obtained in cylindrical shape with a diameter of ½ inch and a thickness of 5 mm. These substrates were subsequently prepared superficially with sandpaper (SiC) of the order 80, 100, 240, 320, 400, 600, 800, 1000 and 1200 μm. After this, they were polished in a metallographic polisher using an alumina water-solution of 1 and 0.3 μm. Finally, an alcohol ultrasound cleaning was carried out using a "Rio Grande UD50SH-2L" equipment for 10 minutes to remove residues on their surface. Monocrystalline silicons with an orientation (100) were also used as substrates. The cathodes used were (Si-N) and (Al-O) both cathodes with a purity of 99.9% obtained from the company "PLASMATERIALS". Argon and Nitrogen were used as precursor gases, both with a purity of 99.9%.

2.2 Coating Deposition

All coatings were deposited on silicon (100) and AISI 316 steel substrates by using a multitarget magnetron reactive sputtering system, with an r.f. source (13.56 MHz) and two targets, Si-N and Al-O with 10 cm of diameter. The deposition parameters used were a sputtering system with one target of Si-N and one of Al-O facing each other, the power applied to the Si-N target was 500W and 400W for the Al-O target; substrate–target distance was 7 cm and substrate temperature 300 ºC. The substrate was under circular rotation with 60 RPM to facilitate the formation of the stoichiometric binary coating. The substrates used presented a disk-type geometry with 2 cm in diameter. The sputtering gas was a mixture of Ar (50 sccm) and N_2 (16 sccm) with a total working pressure of 6×10^{-3} mbar. An unbalanced r.f. bias voltage was applied, generating a negative signal fixed at −20 V. Moreover, the magnetron sputtering system has a substrate positioning system in relation to the target spot and with an opening and closing system that controls the shutters operation. This parameter allowed the varying of the bilayer number (n) ranging from 1, 10, 30, and 70; Therefore, it was possible to change the bilayer period (Λ) for all the coatings due to the increase of the bilayer number while maintaining a constant total coating thickness (2 μm).

2.3 Coating characterization technique

The coating thicknesses were obtained by means of a KLA Tencor D-120 Profilometer by using a step-type configuration where the coatings were deposited on half of the silicon (100) substrate surface. Scans were made in the longitudinal direction, from the deposited zone to the uncoated zone, using the height difference associated to the

different surfaces (coated and uncoated zones), to obtain a reliable result, 4 steps (scans) were performed for each coating, each step was 5 mm in length. X-ray diffraction (XRD) was carried out using a PANalytical X'Pert PRO diffractometer with Cu Kα radiation (λ = 1.5406 Å) at Bragg–Brentano configuration (θ/2θ) in high- angle, using 3 samples for each coating. The bilayer periods of the multilayers were measured using a JSM 6490LV JEOL scanning electron microscope, for this analysis, 3 samples were studied for each coating. An extensive X-ray photoelectron spectroscopy (XPS) study was carried out for the $[Si_3N_4/Al_2O_3]_n$ multilayer coatings. XPS was used on the Si_3N_4 and Al_2O_3 single layers to determine the chemical composition and the bonding of silicon, nitrogen, aluminium and oxygen atoms using an ESCAPHI 5500 monochromatic Al Kα radiation, with a passing energy of 0.1 eV, 3 samples for each coating were used to obtain a reliable result. Roughness and gran size for all coatings were obtained using an atomic force microscope (AFM) from Asylum Research MFP-3D® and calculated by a Scanning Probe Image Processor (SPIP®). This is the standard program for processing and presenting AFM data, becoming the de-facto standard for image processing in nanoscale, for this case, 3 samples were used for each coating were the analyzed surface was 5.0 μm x μm. The mechanical analyses were performed via nanoindentations using an Ubi1-Hysitron device and a diamond Berkovich tip at varying loads. From these measurements, load–penetration depth curves of the multilayer coatings were made and these results were evaluated with the Oliver and Pharr method [21], for each coating, 3 samples were used in which their respective indentation matrices were made, as illustrated in the figure 9. The tribological behavior of the $[Si_3N_4/Al_2O_3]_n$ multilayer systems, was carried out under the ASTM G99-17 [22] standard and using a Microtest MT 4001-98 tribometer with a 6 mm diameter 100Cr6 steel pin as the sliding pattern, the applied load was 5 N in a total length of travel of 300 m, with an angular speed of 160 rpm. The pin-on-disk technique was employed in a non-lubricated and lubricated environment with which the friction coefficient as a function of the sliding distance and the bilayer number was acquired. For the test, 100Cr6 steel balls where used as the counterparts of the tribological pair, since these type of balls allow to simulate a tribological scenario where the surface of a multilayer and the surface of a hardened steel interact, as could happen in an industrial process. As for the lubricant used, this was a FMO 85 AW lubricant from LUBRIPLATE, which can be used in the fabrication processes of food, drinks, pharmaceutical processes and equipment present in places where the possibility of exposure or contact with products in the making exists. To obtain reliable statistical results, 3 samples were analysed for each coating in a lubricated and non-lubricated environment. The scratch test was performed under the ASTM G171-03 [23] standard and the equipment used was a Scratch Test Microtest MTR. The parameters for the test were a sliding distance of 6 mm, a load of 0–90 N and a feed rate of 1.97 mm/min, using 3 samples for each coating to obtain a reliable result. The friction wear images for all the coatings were obtained by using a KLA Tencor D-120 profilometer; the thickness of all the coatings was 2 μm. Moreover, to analyse the wear track, an optical interferometer ZYGO New View 200 was used, for each sample applied in the tribological test.

3. RESULTS AND DISCUSSION

3.1 Structural analysis (DRX)

Figure 1a shows the diffraction patterns corresponding to the $[Si_3N_4/Al_2O_3]n$ multilayers in function the bilayer number. It is clearly seen that as the bilayer number increases, so do the intensities of the preferential orientations (101), (201), (209), (2013), (410) and (317) for 2θ = 33.36°, 40.77°, 54.54°, 64.04°, 66.68° and 76.04°, respectively; indicating that all coatings presented a hexagonal crystal structure with spatial group p63/m. These diffraction patterns are in accordance to the indexing files (JCPDC) 00-009-0259 and 00-002-0921 from the International Center for Diffraction Data (ICDD). This increment of intensity was probably due to a greater number of crystallites that were oriented in said preferential direction, specifically a preferential texturization in the (101) and (209) planes [13]. In the fig. 1b shows a close-up in the (101) plane (greater intensity) corresponding to Si3N4, and the position where the structure would be free of stress (dotted line). It can be seen that as the bilayer number increases, the peaks approach the stress-free position (dotted line), indicating a relaxation of the tensile stresses generated in the deposition process. In the fig. 1c shows a close-up in the (209) plane corresponding to Al_2O_3 and the stress free

position (dotted line). It is revealed that as the bilayer number increases, the peaks move towards higher theta values (shift to the right) indicating an increase in compressive stress within the structure. These stresses will influence an increase in the mechanical properties as corroborated in the figure 10.

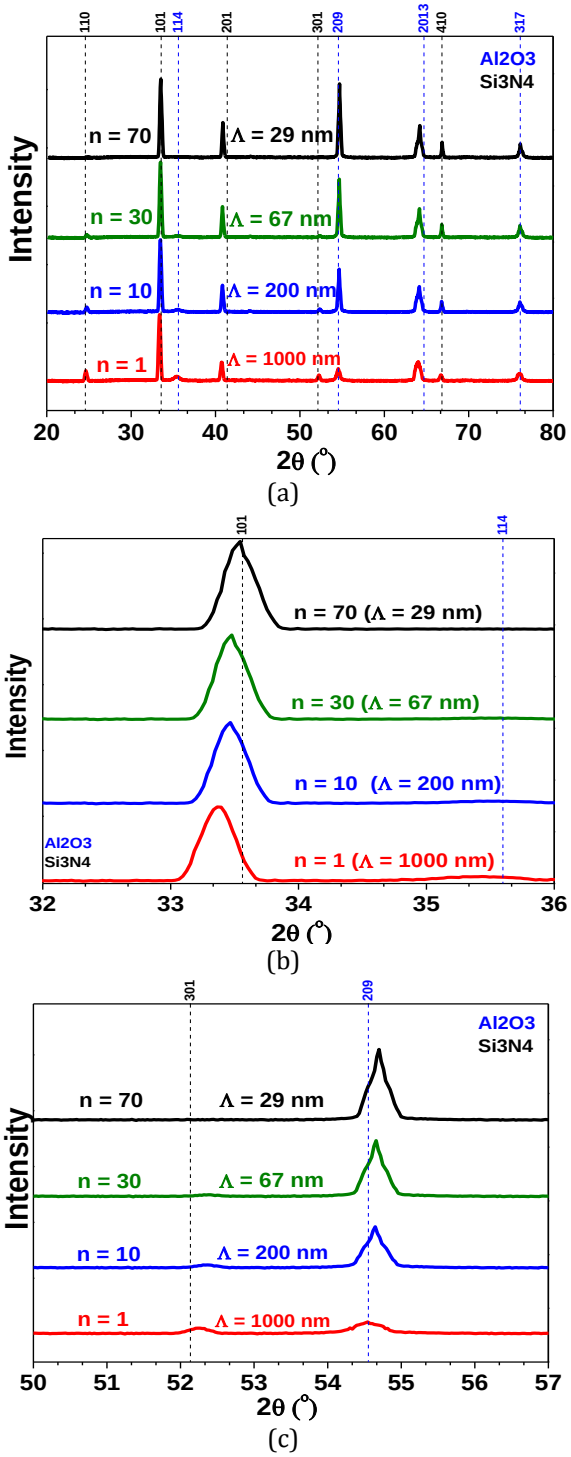

Fig. 1. X-ray diffraction patterns for $[Si_3N_4/Al_2O_3]_n$ multilayers: (a) X-ray diffraction as a function of the bilayers numbers and (b) Close-up for the preferential orientation (101) and (c) (209)

3.2 X-ray Photoelectron Spectroscopy (XPS)

Fig. 2 shows the XPS spectra of the Si_3N_4 coating and details the characteristic intensities of the elements present in the coating, such as Si(2p) and N(1s), but also O(1s), possibly due to sample contamination. Thus, the concentration measurements and the identification of the specific bonding configurations for the Si-N layers are more reliable. Furthermore, the core electronic spectra carry the information of the chemical composition and bonding characters of the Si–N coatings. The integral of the N(1s), and Si(2p) spectra corrected by relevant sensitive factors can evaluate the concentrations of Si, and N elements in the Si-N layer. The corresponding integral of the deconvoluted peaks can also be used to estimate the bond contents, which are described by the following equation (1) [24, 25].

$$C_i = \sum(A_i/S_i)/\sum(A_j/S_{ij}) \quad (1)$$

Where S is the sensitivity factor, A is the integral of the deconvoluted peaks, and C is the atomic content. The numerator is the sum of the integral of one sort of bond; the denominator is the sum of the integral of all types of bonds decomposed from the whole peak of the Si(2p) and N(1s), spectra of the sample. The atomic concentration obtained for the Si-N material were Si_{43}, and N_{57}. For all the Si-N films acquired, the O concentration was less than 2 at.%.

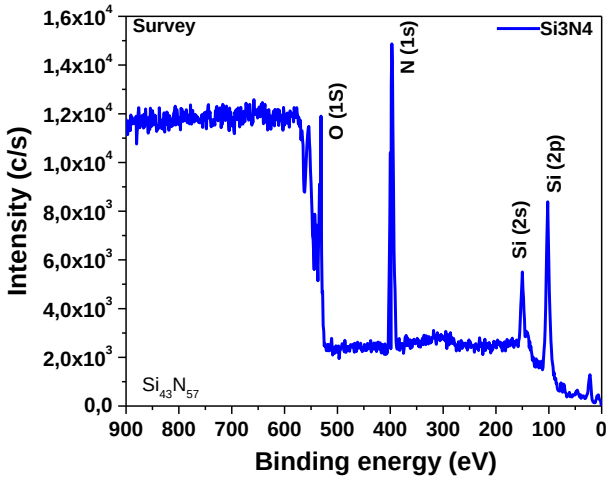

Fig. 2. XPS survey spectrum of the Si–N coating deposited on a Si substrate with an r.f. negative bias voltage of −20 V.

To analyse the detailed superficial stoichiometry of the coating, high-resolution spectra adjusted by Gaussian functions were utilized, shown in Figs. 3a and 3b for N(1s) and Si(2p), respectively. The high-resolution spectra for N(1s) decomposed in three peaks, the first was located at 400.6 eV corresponding to the N-O bond [4, 5]. The second was found at 396.6 eV corresponding to the N-Si bond, and the third peak was situated at 394.4 eV and can be attributed to the different chemical states of N due to its different bond configurations with nearby atoms[6]. Additionally, the high-resolution spectra for Si(2p) only contained two peaks located at 104.88 eV and 101.77 eV, corresponding to the Si-O and Si-N bonds, respectively, in agreements with other author [7, 8].

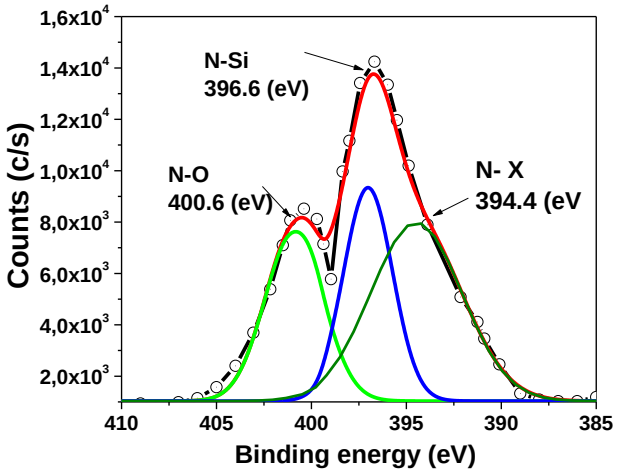

(a) N (1S)

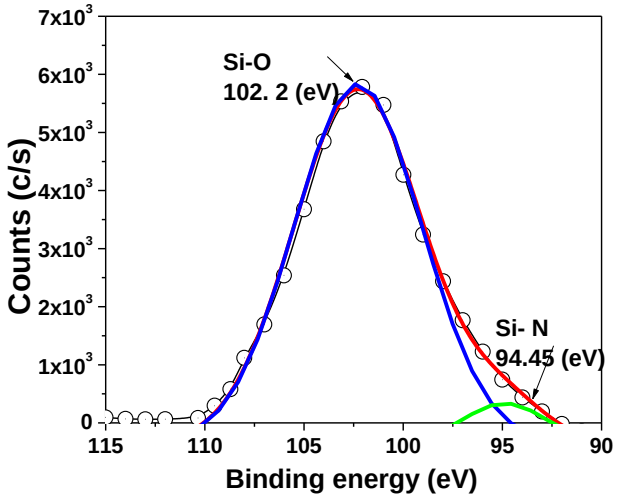

(b) Si (2p)

Fig. 3. High-resolution spectrum of (a) N(1s), and (b) Si(2p) from the Si–N coating.

According to the XPS literature about Al-O materials [13, 26], when the peaks are fitted from experimental results, it is necessary to first adjust the O energy band because it is the element that provides greater reliability for the XPS, then, take that first adjustment as base and, the other peaks related to the remaining elements are adjusted. The latter is indispensable due to the characteristic that is present in this type of insulating materials (coatings) with respect to the incident signal, avoiding the uncertainties caused by charging and shifts of the Fermi energy. Accordingly, Fig. 4 shows the XPS spectra of the Al-O coating, where the intensities for Al(2s), Al(2p) and O(1s) are found. The atomic concentrations obtained from Al-O material were Al_{39}, and O_{61}.

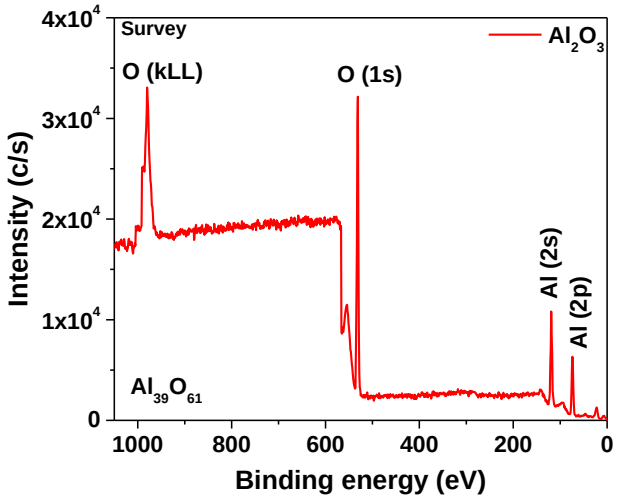

Fig. 4. XPS survey spectrum of Al–O coatings deposited on Si with an r.f. negative bias voltage of −20 V.

As done for the Si_3N_4 coating, high resolution spectra adjusted with Gaussian functions were carried out for Al(2p) and O(1s), which are shown in Fig. 5a and 5b, respectively. Both high resolution spectra for Al(2p) and O(1s) had only one peak, located at 75.9 eV and 532.9 eV, respectively, both attributed to the Al-O bond, surely indicating the presence of Al_2O_3 [10, 13]. On the other hand, the Al(2s) and C(1s) peaks located at 121.09 eV and 254.5 eV can be credited to previous contamination of the sample or test chamber. From these results it was determined that the N/Si and O/Al ratios obtained with these parameters were 1.32 and 1.77 respectively, close to the ideal 1.33 and 1.55 ratios [14, 17].

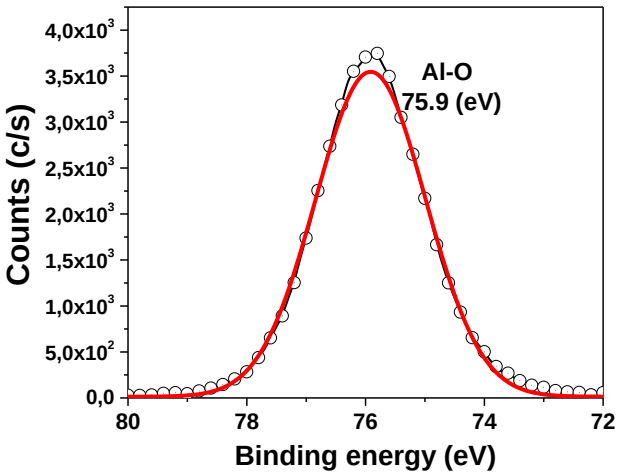

(a) Al(2p)

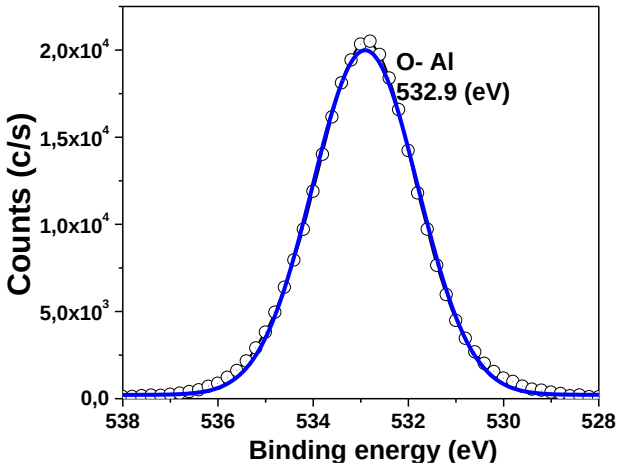

(b) O (1s)

Fig. 5. High-resolution spectrum of (a) A1(2p), and (b) O(1s) from the Al–O coating.

3.3 Scanning Electron Microscopy (SEM)

The Fig 6c, shows the cross section SEM of the $[Si_3N_4/Al_2O_3]_n$ multilayer coating composed by n=10 (Λ = 200 nm) and the fig 6a and 6c show the cross section for Si_3N_4 and Al_2O_3 single layer respectively. The contrast variation seen is due to the difference in the electronic density of both materials; therefore, the lighter contrast corresponds to the Si_3N_4 and the darker contrast corresponds to the Al_2O_3 layer. Consequently, it was determined that the deposited coatings had the configuration as it was designed. In the transversal section of the coating, a dense and continuous morphology can be observed, without visible cracks or deformations, free from the presence of precipitated elements and any other phase in the single layers and multilayer coatings.

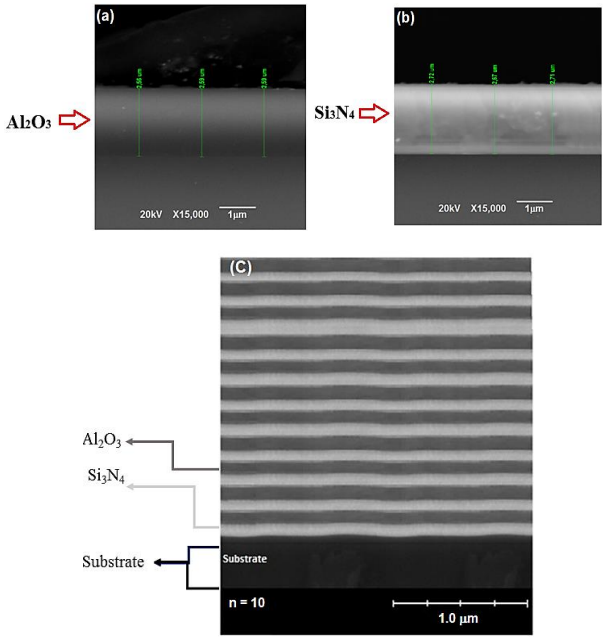

Fig. 6. Cross-sectional SEM micrograph: (a) Si_3N_4 single layer, (b) Al_2O_3 single layer and (c) $[Si_3N_4/Al_2O_3]_n$ multilayer deposited with n = 10.

3.4 Atomic Force Microscopy (AFM)

The atomic force microscopy was performed to study the surface of the multilayer coatings in relation to the bilayers number. Fig. 7 shows the AFM images taken of the $[Si_3N_4/Al_2O_3]_n$ multilayers that were deposited on Si (100) substrates. These images are based on a statistical distribution of grain size carried out in an area of 5x5 µm with a Z-range of 0.5 µm and in no-contact mode for (a) n = 1, Λ = 1000 nm; (b) n = 10, Λ = 200 nm; (c) n = 30, Λ = 67 nm; and (d) n = 70, Λ = 29 nm.

From Fig. 7, the quantitative values of roughness and grain size were obtained using a statistical analysis scanning probe image processor (SPIP®). These values were then plotted as a function of the bilayer number as seen in Fig. 8a and 8b. To ensure that these characteristics were associated to the inherent nature of the system, all the $[Si_3N_4/Al_2O_3]_n$ multilayers were made with a constant total thickness of 2 µm. It is clearly seen that the roughness and surface granule size of the multilayers decreased as the bilayer number increased and the bilayer period decreased, to be precise, a 49.4% and 30.0% reduction, respectively, when comparing the multilayer deposited with n = 1 (Λ = 1000 nm) and n = 70 (Λ = 29 nm). These results also indicate that the multilayer with n = 1 grew more disorderly than the multilayer with n = 70.

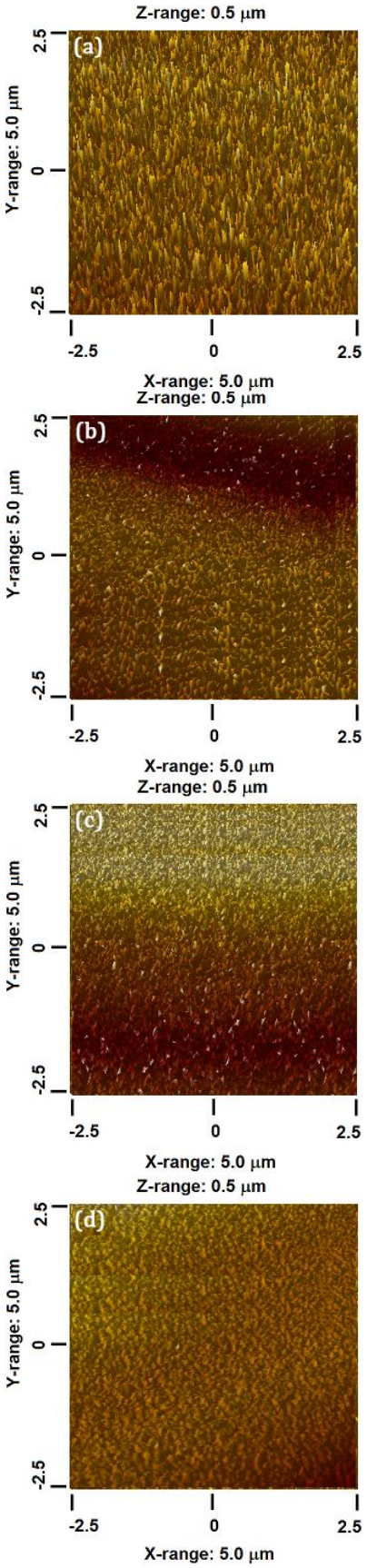

Fig. 7. AFM images of the $[Si_3N_4/Al_2O_3]_n$ multilayer coatings deposited as a function of the bilayer number and bilayer periods (a) n=1, Λ=1000 nm; (b) n=10, Λ=200 nm; (c) n=30, Λ=67 nm; and (d) n=70, Λ=29 nm.

The decrease in grain size was due to nucleation effects caused by different factors, such as the interruption of grain growth when a new layer was deposited, and the reduction of individual coating thicknesses, which stimulated a greater number of nucleation sites. All these aspects caused the microstructure to become more compact and much denser which produce a decrease in the entire surface roughness as well [18]. This last mentioned information is very important because a homogeneous surface can help reduce the corrosion susceptibility of thin films when they are subjected to aggressive environments [19].

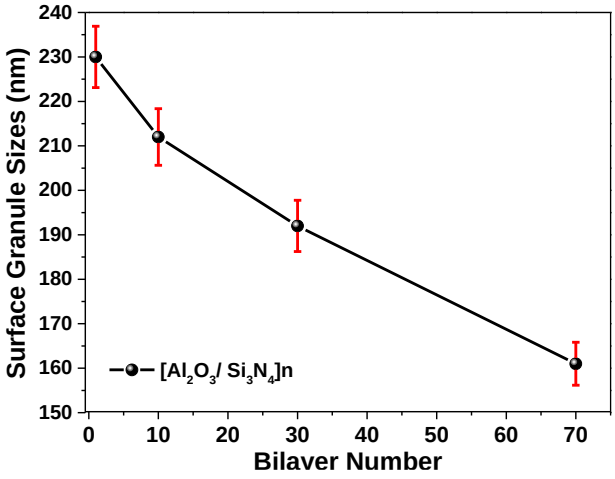

(a)

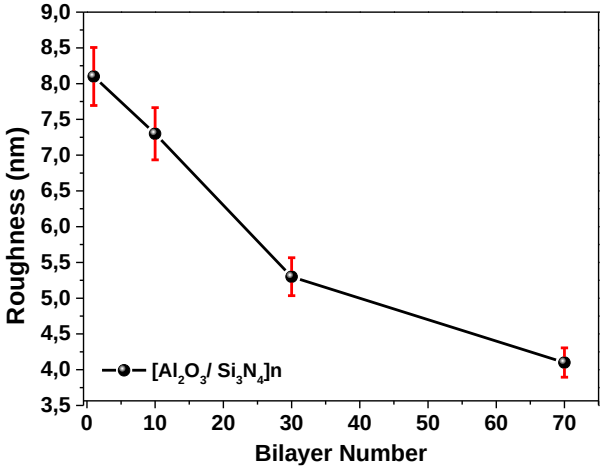

(b)

Fig. 8. Surface analysis (a) Correlation between surface grain size and the bilayer number and (b) correlation between roughness and the bilayer number

3.5 Nanoindentation

Figure. 9a presents the load-displacement curves obtained from the nanoindentation test were a standard *Berkovich* type indenter was used. Moreover, Fig. 9b exhibits the AFM image of the indentation matrix for the multilayer deposited with n = 30 (Λ = 67 nm). The hardness and elastic modulus (Er) were found by using the *Oliver-Pharr* method for the multilayer coatings deposited on the AISI 316 steel substrates [16, 21].

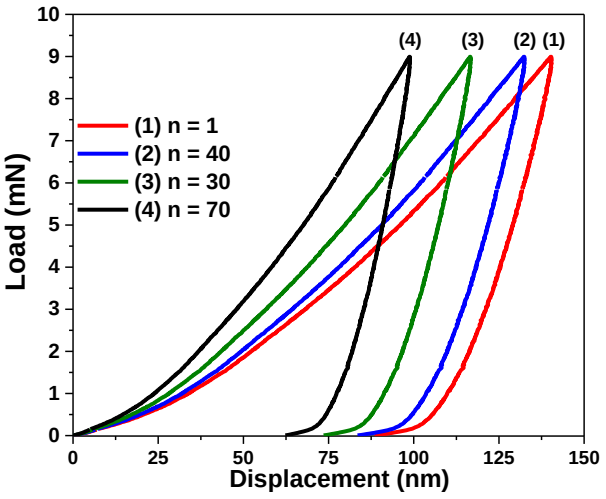

(a)

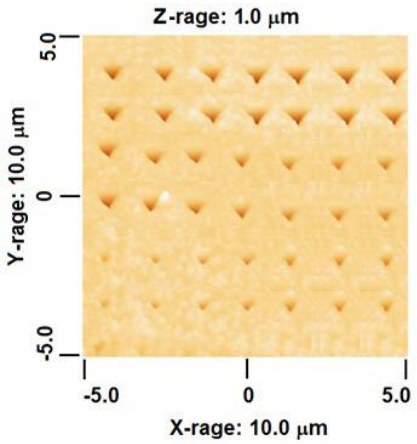

(b)

Fig. 9. Nanoindentation measurements for the $[Si_3N_4/Al_2O_3]_n$ multilayers: (a) load–displacement indentation curves of multilayer coatings, (b) AFM image of the indentation matrix of the multilayer deposited with n = 30 and Λ = 67 nm.

Fig. 10 shows the elastic modulus and hardness that were determined for this study by means of nanoindentation measurements. With the aim that the substrate would not present a contribution to the results, the indentations were made at 10% of the total thickness of the coating. The Hall-Petch effect was used to model the mechanical behavior of the multilayer materials with layer thicknesses between 1-100 nm, modifying the *Hall-Petch* effect in the following equation (2) [20]:

$$H_m = H_{(f1+f2)} + k_{IM} \cdot D_t^{-1/2} \qquad (2)$$

Where H_m is the hardness of the multilayer, $H_{(f1+f2)}$ is the hardness comprised of both layers 1 and 2, K_{IM} is a constant that measures the relative contribution of hardness generated by the thickness of the interface between layers 1 and 2 with units of GPa*m², and D_t is the bilayer period (Λ). The model predicts the global behavior of hardness over the bilayer period, which is observed in many multilayer systems.

As seen in Figs. 10a and 10b, both the elastic modulus and the hardness increased as the bilayer number also increased, obtaining values from 287 GPa at 305 GPa and 31 GPa at 40 GPa, respectively. Presented differently, there was an improvement of 6.3% for the elastic modulus and a 29.0% for the hardness, when comparing the multilayer with n = 70 (Λ = 29 nm) to n=1 (Λ = 1000 nm). This effect is possibly associated to a physical order that is produced by the increase in the quantity of interfaces which block the movement of dislocations between the Si_3N_4 and Al_2O_3 layers because each new interface works as a grain limit, according to the Hall-Petch effect [21]. This impedes the movement of atomic planes and causes the dislocations to gather in or slide through these interfaces since they require a higher critical creep stress related to the differences in shear modulus of the individual materials that form the multilayer coating [27].

Furthermore, this increase in hardness and elastic modulus is also attributable to the reduction of grain size as the bilayer number increases, as seen in the AFM results (Fig. 8). Many studies in the literature revealed the inverse effect that grain size has on the hardness of a coating, affirming that when creating much smaller grains, a larger boundary grain density per unit volume is produced, triggering an obstruction of the dislocations generated by stress, hampering the propagation of cracks and therefore, increasing the hardness and elastic modulus of the coating [15, 16, 27]. Having the previous in mind, a coating with a greater number of interfaces and a smaller grain size, such as the coating with 70 bilayers and with nanometric bilayer period (Λ = 29 nm), will have better mechanical properties [29, 30].

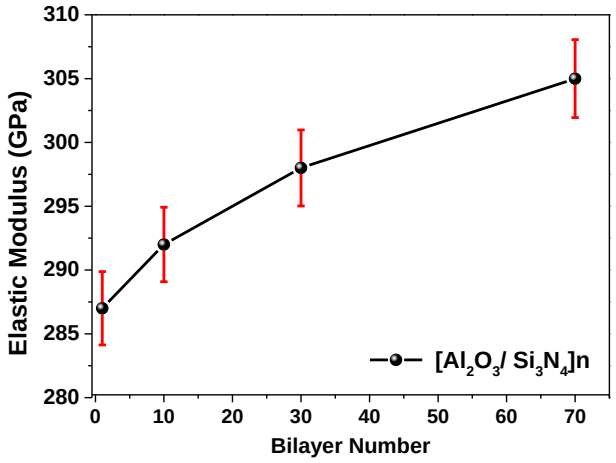

(a)

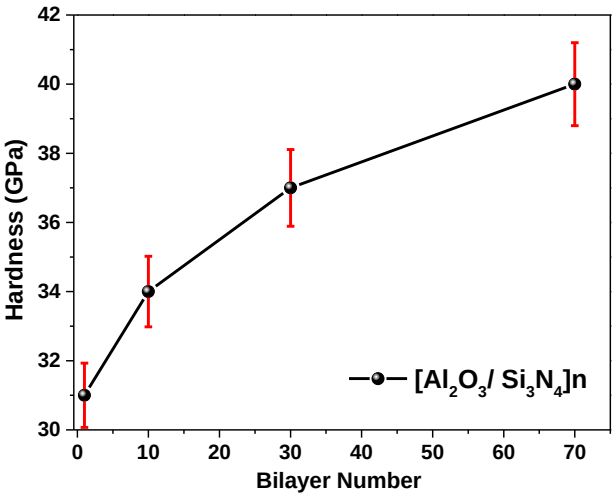

(b)

Fig. 10. Surface properties of the $[Si_3N_4/Al_2O_3]_n$ multilayers: (a) Elastic modulus and (b) Hardness as a function of the bilayer number.

Other properties obtained from the nanoindentation test (load-depth curve) were the plastic deformation resistance (H^3/E^2) and the elastic recovery of the multilayers as a function of the bilayer number, as illustrated in Figs. 11a and 11b, respectively. The elastic recovery was calculated by using the following equation (3):

$$R = \frac{\delta max - \delta p}{\delta max} \quad (3)$$

Where δ_{max} is the maximum displacement (h_{max}) and δp is the residual or plastic displacement (h_f). It can be seen that both the plastic deformation resistance and the elastic recovery increased as the bilayer number (n) did as well, confirming that the multilayer coating with the greatest bilayer number (n = 70) presented the best mechanical properties. This is clearly correlated to the structural coherence found in the XRD results (Fig. 1). Where the preferential texturization and stress relief effect was observed; and the previously mentioned surface properties, such as the increment of the number of interfaces which reduces grain size (Fig. 8), increases grain boundary density and causes an impediment to the movement of microcracks. Thus making it difficult to deform the coating with n = 70 and improving its mechanical properties[16]. This behavior associated to the increase of the mechanical properties was probably due to the lower values of residual stress presented in the multilayers with a higher bilayer number, as seen in the XRD results (Fig. 1).

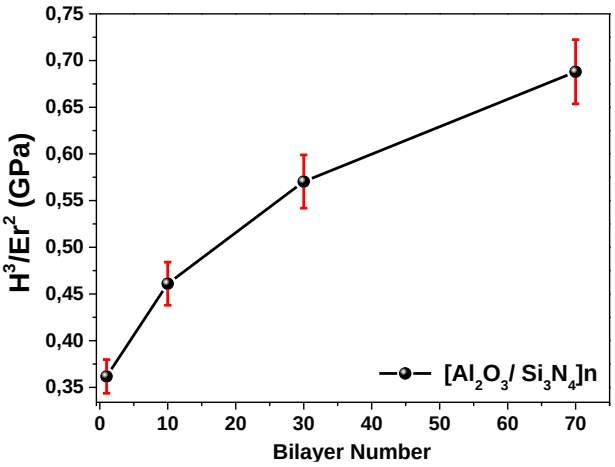

(a)

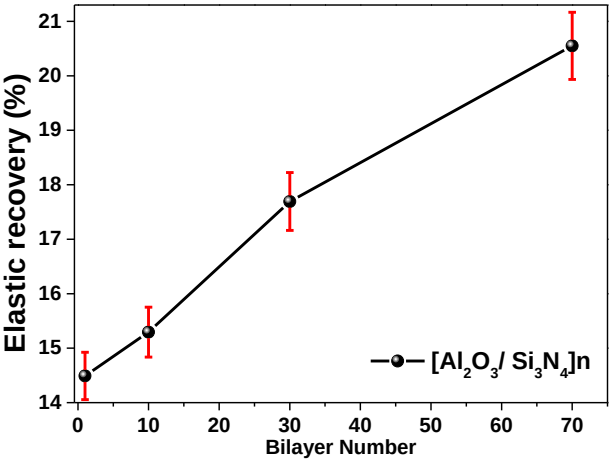

(b)

Fig. 11. Surface properties for the $[Si_3N_4/Al_2O_3]_n$ multilayers coatings: (a) Plastic deformation resistance and (b) Elastic recovery as a function of the bilayer number.

3.6 Pin on disk analysis

To study the tribological behavior of the $[Si_3N_4/Al_2O_3]_n$ multilayer systems, the pin-on-disk technique was employed in a non-lubricated and lubricated environment. Fig. 12 shows the friction coefficient of all multilayers with different bilayer number and the uncoated substrate, where it can be noticed that all the curves presented a two stage behavior in the non-lubricated environment (Fig. 12a). However, the duration of those stages are visibly different for the multilayers with n = 30 and n = 70, possibly due to the grater change in periodicity in comparison to the other coatings when increasing the bilayer number. In stage I, known as the starting period, the friction coefficient begins in low values at first contact, which is associated to the mechanism of interferential friction and is due to the contact between the asperities present among the two surfaces of the tribological pair. Shortly after, the friction coefficient rapidly increases, due to the formation of wear particles called debris. This is later followed by a reduction of the coefficient into a stage of stabilization, caused by the smoothing of the asperities of both surfaces. This stage II, known as *running-in*, is where the annihilation of the asperities is maintained together with the appearance of defects in the coating, associated with the competition between the interferential and adhesive friction mechanisms [30, 31]. Stage II begins at lower sliding distances when the bilayer number increases. This is caused by the fact that the surface with a greater bilayer number has higher mechanical properties and a lower roughness, which generate a lower amount of wear particles in the surface during tribological testing. Therefore, the friction coefficient presents a rapid stabilization in relation to the coatings with lower bilayer number.

Furthermore, when comparing the friction coefficients of the multilayer coatings in a non-lubricated environment to their counterpart in a lubricated environment, a clear difference is observed (Fig. 12b). Not only is the friction coefficient drastically reduced but maintained from an early distance, causing the curves to jump almost immediately to stage II. This is caused by the effective lubrication which lowers the incidence of asperity contact, reduces the surface shear forces, and decreases the wear rate [32]. Again, the multilayer with n = 70 presented the best performance due to its large number of interfaces and the effects that this brings with it. Therefore, the combination of the steels coated with the nanometric $[Si_3N_4/Al_2O_3]_n$ multilayers composed by Si_3N_4 and Al_2O_3 layers and the lubricated environment, offers the best tribological result in the protection of stainless steel devices.

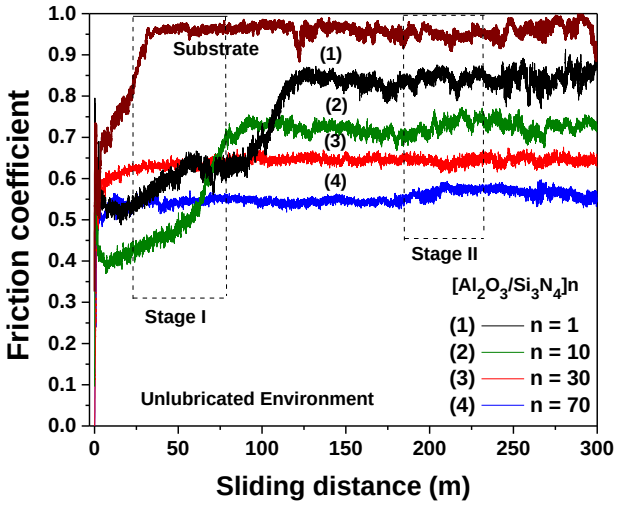

(a)

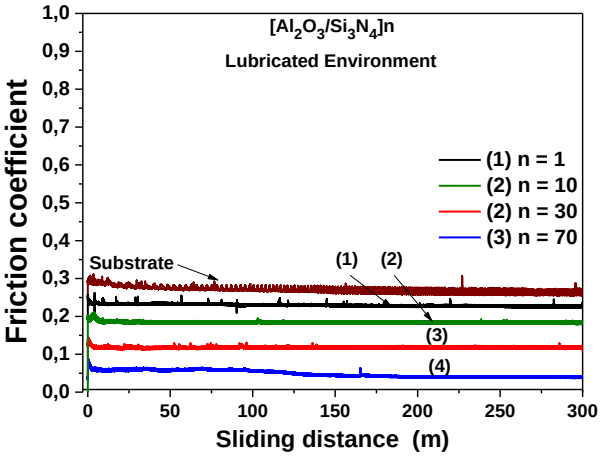

(b)

Figure 12. Friction coefficient as function of sliding distance for all $[Si_3N_4/Al_2O_3]_n$ multilayer coatings (a) Friction coefficient under non-lubricated environment and (b) Friction coefficient under lubricated environment.

Figure 13 shows the progressive decline of the friction coefficient as the bilayer number increases in a non-lubricated environment, indicating that the multilayer deposited with n = 70 (Λ = 29 nm), had the lowest friction

coefficient, giving a reduction of 33.3% when compared to the multilayer with n = 1 (Λ = 1000 nm). This effect might be related to the improvement of the mechanical properties from the interface effect mentioned previously and associated with elastic recovery (Fig. 11); but also, to the mechanical friction model proposed by Archard [33], which relates the contribution of the surfaces in contact (roughness) and the elastic-plastic properties of the coating in the following equation (4):

$$\mu = \frac{F_f}{F_n} = C_k \cdot \frac{R_{(s,a)}}{\sigma t_{(H,Er)}} \quad (4)$$

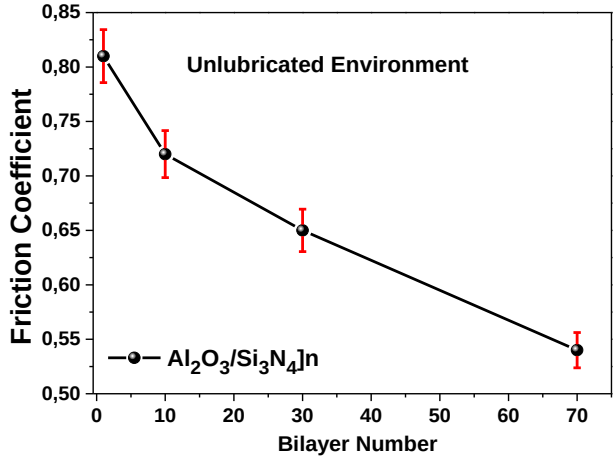

(a)

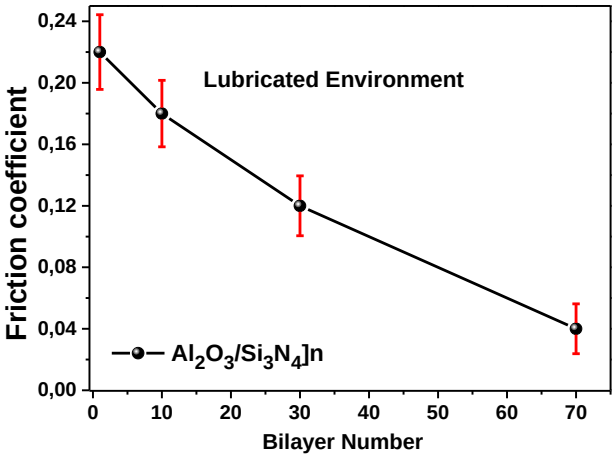

(b)

Figure 13. Friction coefficient as a function of the bilayer number for the $[Si_3N_4/Al_2O_3]_n$ multilayer coatings: (a) non-lubricated environment and (b) Lubricated Environment.

Where, μ is the friction coefficient of the system, *Ck* is a constant that depends on the conditions of the test, *R(s,a)* is the coating's roughness which can be quadratic (for roughness in the order of microns) or arithmetic when the roughness is macroscopic and σ_t is a variable that has in account the elastic-plastic properties of the coating (hardness, H or elastic modulus, E_r). According to Archard's model, when the surface of the coating presents a low roughness (Fig. 8b) and a high hardness (Fig. 10b), the friction coefficient will tend to lower and be stable at prolonged sliding distances, especially if the counterpart of the test is less hard (100Cr6 pin ball) [29, 34]; this seamlessly coincides with the previous results. Moreover, it was possible to analyze the friction coefficient under a lubricated environment (Fig. 13b) where the friction values were reduced to extremely low values thanks to the perfect combination between the multilayers and the lubricant effect.

Additionally, although hardness has been deemed one of the main material properties that correlates to wear resistance, there is compelling data that indicates that the elastic modulus can also have an important effect on the wear behavior. More specifically, the plastic deformation resistance, which is associated with the hardness (H) and the elastic modulus (E) in the form of H^3/E^2 (Fig. 11a), and therefore, the H^3/E^2 relation has been shown by several authors as the most adequate parameter to predict the resistance to wear [30]. The Pin-On-Disk tests was also be used to characterize the wear resistance of the coatings. In addition, the use of scanning electron microscopy (SEM) on the wear track allowed to show the type wear presented on the surface, illustrated in Fig. 14. The nanometric $[Si_3N_4/Al_2O_3]_n$ multilayers presented acceptable results with relatively smooth and continuous wear patterns. It was possible to observe different tribological phenomena present in the wear tracks, for example, wear was evidenced by generated adhesion between the coating surface and the surface of the steel pin (counterpart), which caused a layer delamination. Abrasion was also perceived on the coating surface, generated by particles that delaminated from the coating and from the counterpart that underwent hardening by plastic deformation (debris) [31].

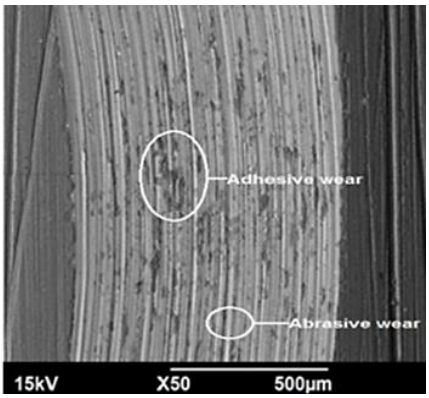

(a) Steel Uncoated

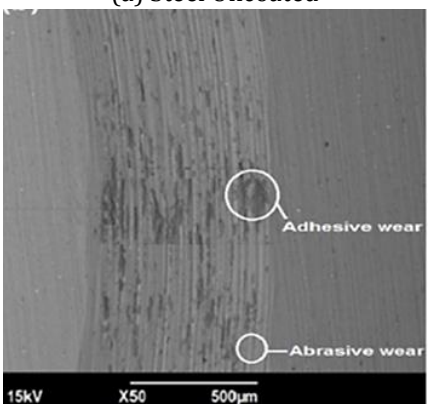

(b) n = 10, Λ = 200

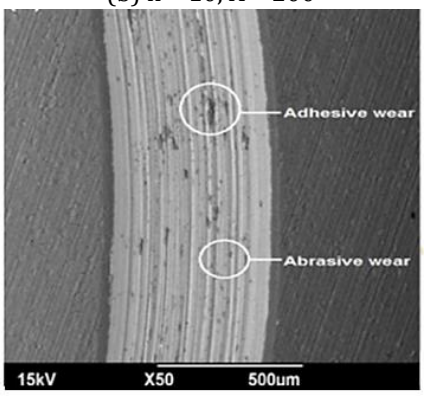

(c) n = 30, Λ = 67 nm

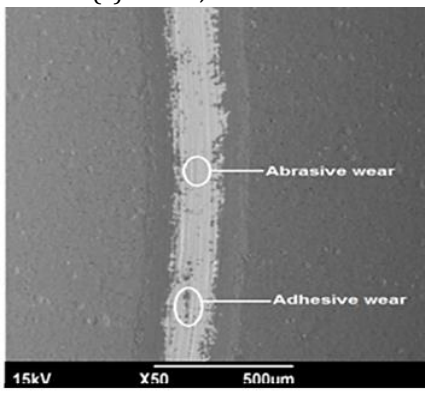

(d) n = 70, Λ = 29 nm

Figure 14. SEM micrographs of the wear tracks after pin-on-disk test for the $[Si_3N_4/Al_2O_3]_n$ multilayer coatings as s function of the bilayer number or bilayer period (Λ): (a) n = 1, Λ = 1000 nm; (b) n = 10, Λ = 200 nm; (c) n = 30, Λ = 67 nm; and (d) n = 70, Λ = 29 nm.

Moreover the multilayer deposited with the least bilayers number (n = 1), which presented the lowest mechanical properties in relation to the multilayers with a high number of bilayers, showed a deeper and wider wear track in comparison to the others, as well as behavior that reflects an abrupt rupture of the material. These types of traces are generally associated with the adhesion and abrasion mechanisms mentioned. On the other hand, the multilayers with a high bilayers number (n) or low periodicity (Λ) showed a completely different behavior; a decrease of wear and track size was observed when the number of bilayers increased, confirming the effect that the number of layers exerts against wear resistance. Therefore, the best wear performance in dynamic mode against 100Cr6 steel balls (counterpart) was presented by the multi-layer with n = 70 (Λ = 29 nm), due to the combination of a low friction coefficient, low roughness and high hardness obtained thanks to the multi-layer structure with a high number of interfaces.

Figure 15 shows the 3D profiles of the wear tracks. It is possible to observe the difference in wear in the non-lubricated environment when the bilayer number increases. Additionally, as the mechanical properties increased, the friction coefficient decreased and the coating resistance increased, showing a reduction in depth and width of the track.

Fig. 16 presents the values of the track width and track depth generated during the tribological test for the $[Si_3N_4/Al_2O_3]_n$ multilayer coating as a function of the bilayer number. In these results it is possible to observe the geometrical wear reduction when the mechanical properties (Figs. 10-11) are improved such as elastic modulus and plastic deformation resistance which reduce the possibility of generating microcracks and minimize the delamination mechanisms. Therefore, the coating with the lowest number of bilayers (n = 1, Λ = 1000 nm) had the greatest wear effect, with an average track width of 3.03 mm and depth of 2.36 µm, while the coating with the highest bilayer number n = 70, (Λ = 29 nm) had the least wear with a track width of 1.12 mm and depth of 0.215 µm, as shown in Figs. 16a and 16b, demonstrating a reduction of 63.0% and 91.2%, respectively.

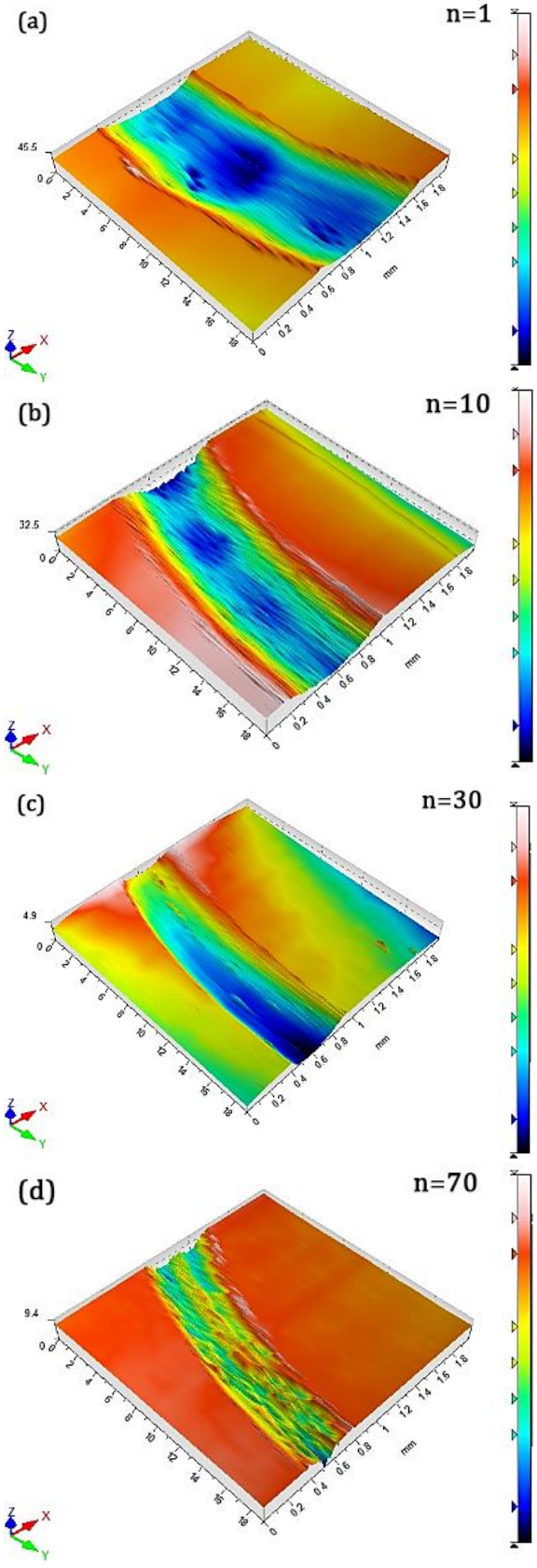

Fig. 15. 3D profiling images of the wear tracks after the pin-on-disk test for the $[Si_3N_4/Al_2O_3]_n$ multilayers coating as a function of the bilayer number: (a) n = 1, Λ = 1000 nm; (b) n = 10, Λ = 200 nm; (c) n = 30, Λ = 67 nm; and (d) n = 70, Λ = 29 nm.

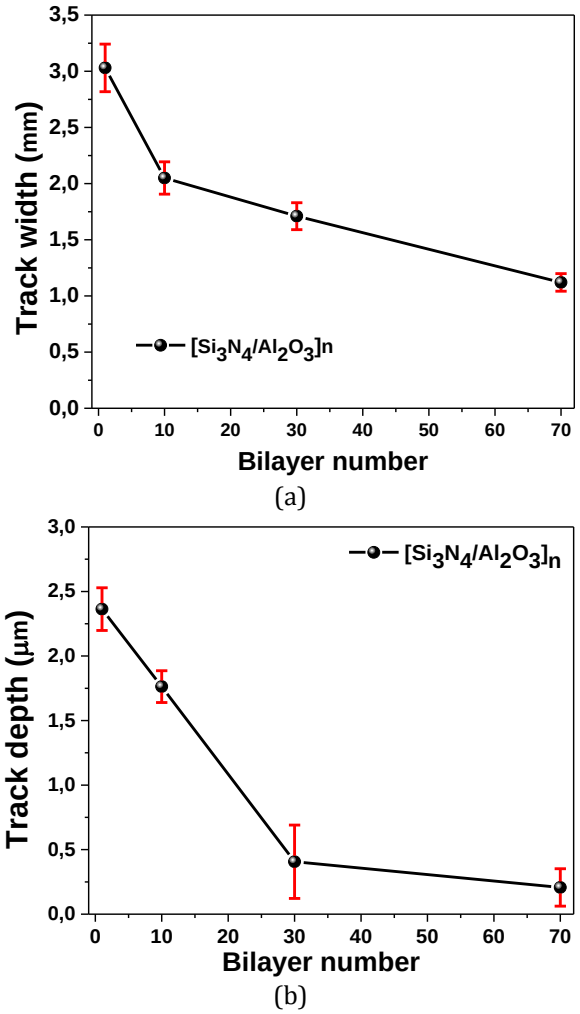

Fig. 16. Geometrical measurements of the wear tracks after the pin-on-disk test for the $[Si_3N_4/Al_2O_3]_n$ multilayers coatings as a function of the bilayer number: (a) Track width and (b) Track depth.

3.7 Scratch test analysis

To characterize the adhesion properties of the nanocomposite $[Si_3N_4/Al_2O_3]_n$ multilayer coatings the scratch test was carried out. Fig. 17 presents the results of the scratch test for all multilayers. Taking into account that the adhesion properties are characterized by two terms, L_{C1}, being the low critical load where the first cracks are produced by the cohesive failure; and L_{C2}, being the superior critical load where the first delamination in the border of the scratch mark takes place by means of the adhesive failure. The different critical loads were determined from the regions where the load becomes independent from the friction coefficient, meaning where the load stabilizes with respect to the friction coefficient in the curve. The first stabilization is credited to the cohesive failure, while the second stabilization is credited to the adhesive failure [33-37].

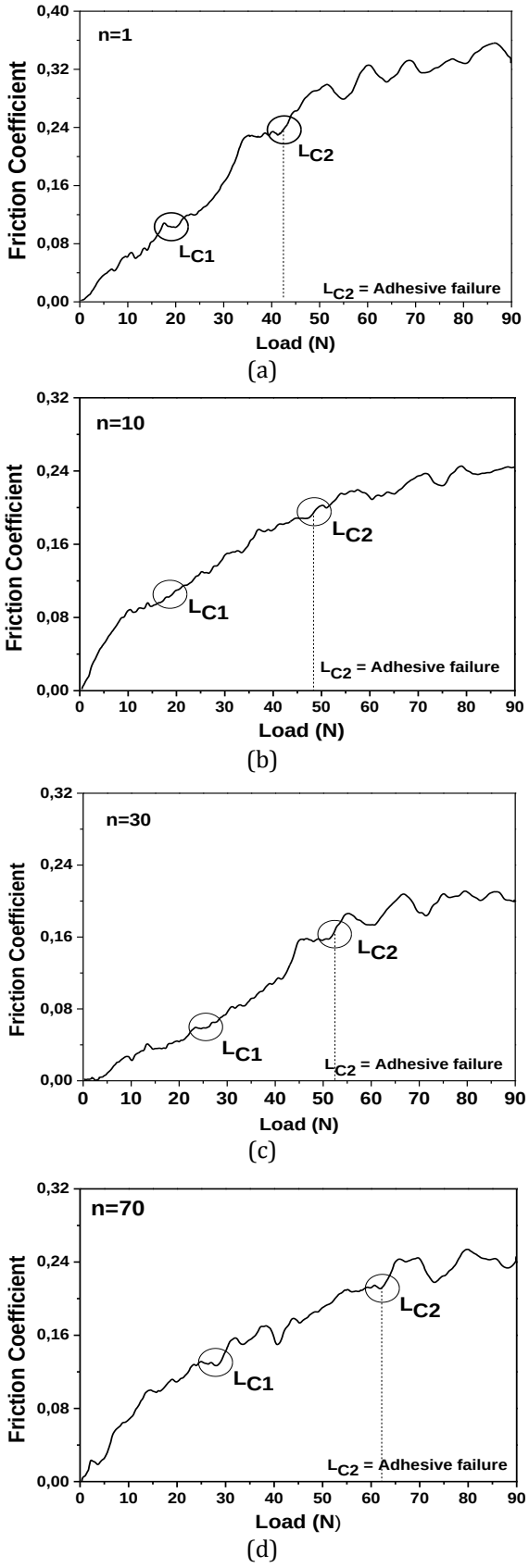

Fig. 17. Friction coefficient as a function of the applied load obtained from the scratch test results for all $[Si_3N_4/Al_2O_3]_n$ multilayer coatings: (a) n = 1, Λ = 1000 nm; (b) n = 10, Λ = 200 nm; (c) n = 30, Λ = 67 nm; and (d) n = 70, Λ = 9 nm.

From the data obtained from figure 17, the Fig. 18 was made, showing how the superior critical load (L_{C2}) differs as the bilayer number changes. As seen, a greater critical load was needed for the adhesive failure to occur as the bilayers number increased; which means that the multilayer with n = 70 (Λ = 29 nm), presented the best multilayer adhesion in comparison to the other $[Si_3N_4/Al_2O_3]_n$ multilayer, with a critical load of 62 N, obtaining a 47.6% increase when compared to n = 1 (Λ = 1000 nm). This behavior was probably due to the lower values of residual stress in the multilayers with a higher bilayer number, as seen in the XRD results (Fig. 1).

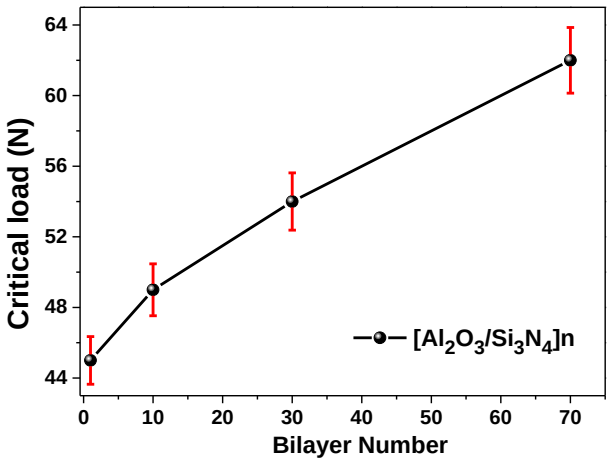

Fig. 18. Critical load as a function of the bilayer number for the $[Si_3N_4/Al_2O_3]_n$ multilayer coatings.

CONCLUSIONS

- The structural analysis determined that the multilayer coatings $[Si_3N_4/Al_2O_3]n$ presented a hexagonal crystalline structure with preferential orientations (101) and (209) for the Si_3N_4 and Al_2O_3 layers respectively.
- AFM results indicated a reduction of grain size and roughness of approximately 30.0% and 49.4%, respectively, when increasing the bilayer number from n = 1 to n = 70.
- The multilayer with the highest bilayer number (n = 70) and lowest bilayer period (Λ = 200) obtained a hardness of 40 GPa and an elastic modulus of 305 GPa, showing a 29.0% and 6.3% improvement, respectively, when comparing to the multilayer with the lowest bilayer number (n = 1).

- Tribological results show an approximate 33.3% decrease in friction coefficient (0.54) within a non-lubricated environment and 81.8% decrease in friction coefficient under lubricated environment for the multilayer with the highest bilayer number (n = 70) when compared to the lowest (n = 1),

- Scratch results showed a 47.61% increase in critical load was needed for adhesive failure, indicating that these multilayer coatings may be a promising material to be applied in the food and pharmaceutical industries.

Acknowledgement

This research was supported by the Universidad del Valle through project number C.I 21024 and Centro de Desarrollo Tecnológico y Asistencia Técnica a la Industria Del Servicio Nacional de Aprendizaje (CDT-ASTIN SENA), Regional Valle, Cali-Colombia; CINVESTAV, Mexico; Universitat de Barcelona, Catalunya, Spain; the Excellence Center for Novel Materials (CENM) at Universidad del Valle in Colombia, under Contract RC- 043-2005 with Colciencias and Vicerrectoría de investigaciones de la Universidad Militar Nueva Granada" under contract ING- 2374 - 2017.

REFERENCES

[1] C.H. Ortiz, H.D. Colorado, W. Aperador, A. Jurado, *Influence of the number of bilayers on the mechanical and tribological properties in [TiN/TiCrN]n multilayer coatings deposited by magnetron sputtering*, Tribology in Industry, vol. 41, no. 3, pp. 330–343, 2019, doi: 10.24874/ti.2019.41.03.03

[2] D.D. Kumar, N. Kumar, S. Kalaiselvam, S. Dash, R. Jayavel, *Wear resistant super-hard multilayer transition metal-nitride coatings*, Surfaces and Interfaces, vol. 7, pp. 74–82, 2017, doi: 10.1016/j.surfin.2017.03.001

[3] J.C. Caicedo, A. Guerrero, W. Aperador, *Determination of multilayer effect evidence on metal carbon-nitride system*, Journal of Alloys and Compounds, vol. 785, pp. 178–190, 2019, doi: 10.1016/j.jallcom.2019.01.151

[4] K. Kishi, M.W. Roberts, *Adsorption of nitrogen and ammonia by polycrystalline iron surfaces in the temperature range 80–290 K studied by electron spectroscopy*, Surface Science, vol. 62, iss. 1, pp. 252–266, 1977, doi: 10.1016/0039-6028(77)90441-1

[5] V. Bonu, M. Jeevitha, V. Praveen Kumar, G. Srinivas, Siju, H.C. Barshilia, *Solid particle erosion and corrosion resistance performance of nanolayered multilayered Ti/TiN and TiAl/TiAlN coatings deposited on Ti6Al4V substrates*, Surface and Coatings Technology, vol. 387, pp. 125531, 2020, doi: 10.1016/j.surfcoat.2020.125531

[6] S.H. Shin, J.W. Cho, S.H. Kim, *Structural investigations of CaO-CaF2-SiO2-Si3N4 based glasses by Raman spectroscopy and XPS considering its application to continuous casting of steels*, Materials and Design, vol. 76, pp. 1–8, 2015, doi: 10.1016/j.matdes.2015.03.035

[7] S. Yadav, S. Sahoo, *Interface study of thermally driven chemical kinetics involved in Ti/Si3N4 based metal-substrate assembly by X-ray photoelectron spectroscopy*, Applied Surface Science, 2020, doi: 10.1016/j.apsusc.2020.148465

[8] M. Pettersson, M. Bryant, S. Schmidt, H. Engqvist, R.M. Hall, A. Neville, C. Persson, *Dissolution behaviour of silicon nitride coatings for joint replacements*, Materials Science and Engineering: C, vol. 62, pp. 497–505, 2016, doi: 10.1016/j.msec.2016.01.049

[9] P.H.C. Camargo, K.G. Satyanarayana, F. Wypych, *Nanocomposites: Synthesis, structure, properties and new application opportunities*, Materials Research, vol. 12, no. 1, pp. 1–39, 2009, doi: 10.1590/S1516-14392009000100002

[10] A. Pogrebnjak, K. Smyrnova, O. Bondar, *Nanocomposite Multilayer Binary Nitride Coatings Based on Transition and Refractory Metals, Structure and Properties*, Coatings, vol. 9, iss. 3, pp. 155, 2019, doi: 10.3390/coatings9030155

[11] S. Zimowski, T. Moskalewicz, B.G. Wendler, *Analysis of the tribological properties of TiN/Si3N4 nanocomposite coating in sliding contact with ceramic, steel, and polymer counterpart*, Tribologia, vol. 4, pp. 125, 2017.

[12] I. Mohammadi, A. Afshar, S. Ahmadi, *Al2O3/Si3N4 nanocomposite coating on aluminum alloy by the anodizing route: Fabrication, characterization, mechanical properties and electrochemical behavior*, Ceramics International, vol. 42, iss. 10, pp. 12105–12114, 2016, doi: 10.1016/j.ceramint.2016.04.142

[13] M. Michalak, L. Łatka, P. Sokołowski, A. Niemiec, A. Ambroziak, *The microstructure and selected mechanical properties of Al2O3 + 13 wt % TiO2 plasma sprayed coatings*, Coatings, vol. 10, iss. 2, 39–45, 2020, doi: 10.3390/coatings10020173

[14] C. Escobar, M. Villarreal, J.C. Caicedo, W. Aperador, H.H. Caicedo, P. Prieto, *Diagnostic of corrosion-erosion evolution for [Hf-Nitrides/V-Nitrides]n structures*, Thin Solid Films, vol. 545, pp. 194–199, 2013, doi: 10.1016/j.tsf.2013.07.081

[15] G. Pradhaban, P. Kuppusami, D. Ramachandran, K. Viswanathan, R. Ramaseshan, *Nanomechanical properties of TiN/ZrN multilayers prepared by pulsed laser deposition*, Materials Today: Proceedings, vol. 3, iss. 6, pp. 1627–1632, 2016, doi: 10.1016/j.matpr.2016.04.052

[16] J.C. Caicedo, G. Cabrera, H.H. Caicedo, C.Amaya, W. Aperador, *Nature in corrosion-erosion surface for [TiN/TiAlN]n nanometric multilayers growth on AISI 1045 steel*, Thin Solid Films, vol. 520, iss. 13, pp. 4350–4361, 2012, doi: 10.1016/j.tsf.2012.02.061

[17] S. Prasanna, G. Krishnendu, S. Shalini, P. Biji, G. Mohan Rao, S. Jayakumar, R. Balasundaraprabhu, *Materials Science in Semiconductor Processing Composition, structure and electrical properties of DC reactive magnetron sputtered Al2O3 thin films*, Materials Science in Semiconductor Processing, vol. 16, iss. 3, pp. 705–711, 2013, doi: 10.1016/j.mssp.2012.12.012

[18] S. Prasanna, G. Krishnendu, S. Shalini, P. Biji, G.M. Rao, S. Jayakumar, R. Balasundaraprabhu, *Composition, structure and electrical properties of DC reactive magnetron sputtered Al2O3 thin films*, Materials Science in Semiconductor Processing, vol. 16, iss. 3, pp. 705–711, 2013, doi: 10.1016/j.mssp.2012.12.012

[19] A.A. Pradhan, S.I. Shah, K.M. Unruh, *Reactive sputter deposition of alumina thin films using a hollow cathode sputtering source*, Review of Scientific Instruments, vol. 73, iss. 11, pp. 3841–3845, 2002, doi: 10.1063/1.1512340

[20] J.C. Caicedo, G . Bejarano, M.E. Gómez, P. Prieto, C. Cortéz, J. Muñoz, *Nanostructured multilayers of TiN/ZrN obtained by magnetron sputtering*, Physica Status Solidi C, vol. 4, iss. 11, pp. 4127–4133, 2007, doi: 10.1002/pssc.200675912

[21] Y.W. Bao, W. Wang, Y.C. Zhou, *Investigation of the relationship between elastic modulus and hardness based on depth-sensing indentation measurements*, Acta Materiala, vol. 52, iss. 18, pp. 5397–5404, 2004, doi: 10.1016/j.actamat.2004.08.002

[22] ASTM G99-17, *Standard Test Method for Wear Testing with a Pin-on-Disk Apparatus,* 2017.

[23] ASTM G171–03, *Standard Test Method for Scratch Hardness of Materials Using a Diamond Stylus*, 2003.

[24] I. Iatsunskyi, M. Kempiński, M. Jancelewicz, K. Załęski, S. Jurga, V. Smyntyna, *Structural and XPS characterization of ALD Al2O3 coated porous silicon*, Vacuum, vol. 113, pp. 52–58, 2015, doi: 10.1016/j.vacuum.2014.12.015

[25] C. Zhuang, J. Zhao, F. Jia, C. Guan, Z. Wu, Y. Bai, X. Jiang, *Tuning bond contents in B–C–N films via temperature and bias voltage within RF magnetron sputtering*, Surface and Coatings Technology, vol. 204, iss. 5, pp. 713–717, 2009, doi: 10.1016/j.surfcoat.2009.09.031

[26] C. Zhuang, J. Zhao, F. Jia, C. Guan, Z. Wu, Y. Bai, X. Jiang, *Tuning bond contents in B–C–N films via temperature and bias voltage within RF magnetron sputtering*, Surface and Coatings Technology, vol. 204, iss. 5, pp. 713–717, 2009, doi: 10.1016/j.surfcoat.2009.09.031

[27] A.A. Vereschaka, S.N. Grigoriev, *Study of cracking mechanisms in multi-layered composite nano-structured coatings*, Wear, vol. 378–379, pp. 43–57, 2017, doi: 10.1016/j.wear.2017.01.101

[28] S. Nikkhah, H. Mirzadeh, M. Zamani, *Improved mechanical properties of mild steel via combination of deformation, intercritical annealing, and quench aging*, Materials Science and Engineering A, vol. 756, pp. 268–271, 2019, doi: 10.1016/j.msea.2019.04.071

[29] Z.B. Qi, P. Sun, F.P. Zhu, Z.C. Wang, D.L. Peng, C.H. Wu, *The inverse Hall-Petch effect in nanocrystalline ZrN coatings*, Surface and Coatings Technology, vol. 205, iss. 12, pp. 3692–3697, 2011, doi: 10.1016/j.surfcoat.2011.01.021

[30] L. Ipaz, J.C. Caicedo, J. Esteve, F.J. Espinoza-Beltran, G. Zambrano, *Improvement of mechanical and tribological properties in steel surfaces by using titanium-aluminum/titanium-aluminum nitride multilayered system*, Applied Surface Science, vol. 258, iss. 8, pp. 3805–3814, 2012, doi: 10.1016/j.apsusc.2011.12.033

[31] S.-K. Tien, J.-G. Duh, *Effect of heat treatment on mechanical properties and microstructure of CrN/AlN multilayer coatings*, Thin Solid Films, vol. 494, iss. 1-2, pp. 173–178, 2006, doi: 10.1016/j.tsf.2005.08.198

[32] I. Hutchings, P. Shipway, *Sliding wear*, Tribology: Friction and Wear of Engineering Materials, pp. 107–164, 2017, doi:10.1016/B978-0-08-100910-9.00005-2

[33] J. Sunil, J. Godwin, C.M. Selvam, *Roles of nanomaterials at the rubbing interface of mechanical systems*, Materials Today: Proceedings, vol. 21, pp. 184–188, 2020, doi: 10.1016/j.matpr.2019.04.218

[34] W.F. Piedrahita, W. Aperador, J.C. Caicedo, P. Prieto, *Evolution of physical properties in hafnium carbonitride thin films*, Journal of Alloys and Compounds, vol. 690, pp. 485–496, 2017, doi: 10.1016/j.jallcom.2016.08.109

[35] K.N. Andersen, E.J. Bienk, K.O. Schweitz, H. Reitz, J. Chevallier, P. Kringhøj, J. Bøttiger, *Deposition, microstructure and mechanical and tribological properties of magnetron sputtered TiN/TiAlN multilayers*, Surface and Coatings Technology, vol. 123, iss. 2–3, pp. 219–226, 2000, doi: 10.1016/S0257-8972(99)00473-9

[36] A. Leyland, A. Matthews, *On the significance of the H/E ratio in wear control: a nanocomposite coating approach to optimised tribological behaviour*, Wear, vol. 246, iss. 1–2, pp. 1–11, 2000, doi: 10.1016/S0043-1648(00)00488-9.

[37] M. Falsafein, F. Ashrafizadeh, A. Kheirandish, *Influence of thickness on adhesion of nanostructured multilayer CrN/CrAlN coatings to stainless steel substrate*, Surfaces and Interfaces, vol. 13, pp. 178–185, 2018, doi: 10.1016/j.surfin.2018.09.009